African Journal of Pure & Applied Sciences

ISSN: 2710-0758
DOI 10.33886/ajpas.v4i3.426

Journal homepage: http://journal.ku.ac.ke/index.php/AJPAS

Research Article Open Access

Characterization of amorphous silicon nitride prepared from sand and coffee husk wastes by carbothermal reduction-nitridation

Ndung'u S.N.[1*], Nthiga E.W.[2], Wanjau R.N.[1]

[1]Department of Chemistry, Kenyatta University, P.O Box 43844-00100, Nairobi, Kenya.
[2]Department of Chemistry, Dedan Kimathi University of Technology, P.O Box 657-10100, Nyeri, Kenya.
[1*]Corresponding author: samuelndungu530@gmail.com, samuelndungu53@yahoo.com

Received 8th July , 2023/ Accepted 9th Sept2023, Published online 31st December, 2023

How to cite:
Ndung'u, S., Nthiga, E., & Wanjau, R. (2023). Characterization of amorphous silicon nitride prepared from sand and coffee husk wastes by carbothermal reduction-nitridation. *African Journal of Pure and Applied Sciences,* 4(3), i-j. https://doi.org/10.33886/ajpas.v4i3.426

ABSTRACT

The continued coffee demand in Kenya has amplified the generation of its husk wastes causing disposal problems. This has led to serious pollution to the environment. Therefore, developing a greener and cost-effective ways to handle these wastes is necessary. The current study entailed the use of extracted silica and coffee husk biochar as novel precursor materials for the synthesis of silicon nitride (Si_3N_4) composite in an ammonia environment. The silica was extracted from raw sand by alkali fusion route. The biochar was prepared by pyrolytic treatment of raw coffee husk biomass at 300 °C for 5 hours followed by acid leaching. The sand, extracted silica, raw and biochar samples and silicon nitride composites were characterized using X-Ray Fluorescence (XRF), Fourier Transform Infrared (FT-IR), X-Ray Diffractometer (XRD), Scanning Electron Microscope (SEM), Energy Dispersive X-Ray (EDX) and Thermogravimetric Analyzer (TGA). The results showed that the raw sand contain quartz, calcite, microcline and clinochlore. The results for the extracted silica showed a highly amorphous silica containing hydroxyl (-OH) and siloxane (Si-O-Si) functional groups. The alkali fusion process increased the silica content to > 92 % from 83 % with oxide impurities reduced to < 1 %. The characterization of biochar samples showed a highly amorphous, porous carbon structure with aromatic carbon bonds (C=C) and a negligible ash content. The characterization of Si_3N_4 powder showed thermally stable, porous and highly amorphous material with α-Si_3N_4 and α- Si_3N_4 phases. The FT-IR results showed Silicon-Nitrogen-Silicon (Si-N-Si), silanol (Si-OH), Silicon-Nitrogen (Si-N) and Silicon-Silicon (Si-Si) as important functional groups present in silicon nitride composite material. The results revealed a greener approach of Si_3N_4 synthesis for application in vast industrial fields.

Key words: Extracted silica (ES), Silicon nitride (Si_3N_4), Bamburi Beach Sand (BBS), Coffee husk biochar (CHB), α- Si_3N_4, β- Si_3N_4

INTRODUCTION

Silicon nitride material is employed in vast fields due to its outstanding thermomechanical properties, corrosion resistance, high thermal conductivity and chemical inertness amongst others (Pan, 2014). The structure has a rigid structure with strong covalent bonds (Sharma *et al.,* 2018). These features make the material suitable in many applications such as in optoelectronic devices, automotive engine parts, nanocomposites and ball bearings amongst others (Farzana *et al.,* 2018). Silicon nitride occurs in two phases, an alpha (α) form (trigonal) which is stable at lower temperatures and a beta (β) form (hexagonal) stable at higher temperatures (Parrillo *et al.,* 2021).

Various techniques such as metallurgy method (Tran *et al.,* 2021), oxide-assisted growth (Zhao *et al.,* 2021), direct nitridation of silicon (Jin *et al.,* 2019), electrochemical method (Vishnu *et al.,* 2018), chemical vapour deposition (Liu *et al.,* 2018) and carbothermal reduction-nitridation of amorphous silica (Abdulhameed *et al.,* 2018) among

others are reported for Si_3N_4 synthesis. Carbothermal reduction-nitridation is the most cost-effective for a large-scale synthesis (Ji *et al.,* 2014). This is because it utilizes vast low-cost materials for the Si_3N_4 synthesis (Rajarao and Veena, 2016). The synthesis is carried out in an ammonia (NH_3) environment as shown in Equation 1 (Xiaohan, 2013).

$$3SiO_{2(s)} + 6C_{(s)} + 4NH_{3(g)} \longrightarrow Si_3N_{4(s)} + 6CO_{(g)} + 6H_{2(g)} \quad (1)$$

Various researches have been reported on the synthesis of Si_3N_4 using locally available wastes such as silica fumes (Ji *et al.,* 2014), rice husk (Parrillo *et al.,* 2021) and wheat husk (Qadri *et al.,* 2016) amongst others. Amorphous silica is widely used in vast fields such as in waste water treatment, cosmetics, electronics, paint, textiles, rubber, paper and concrete ceramics amongst others (Wahyudi *et al.,* 2013; Setyoningrum *et al.,* 2020). It can be extracted from agricultural wastes, natural minerals and biogenic marine organisms such as bagasse ash (Norsuraya *et al.,* 2016; Megawati *et al.,* 2018), beach sand (Eddy *et al.,* 2015), coconut pulp (Anuar *et al.,* 2018), rice husk ash (Bakar *et al.,* 2016) and fly ash (a coal waste) (Cheng *et al.,* 2018) amongst others. Silica sand is reported to contain active silica from silica-silicate minerals which are potential for chemical dissolution via alkali-silica reactions (Hasdemir *et al.,* 2012). The objective of the study entailed alkali fusion silica extraction from sand, biochar preparation from coffee husk wastes and utilize the materials for the synthesis of Si_3N_4 in an ammonia environment.

MATERIAL AND METHODS

Chemicals and reagents

Analar (> 99.5% purity) grade chemicals and reagents were used in this study. Sodium hydroxide (NaOH), Hydrochloric acid (HCl), Ammonium solution (NH_4OH) and Nitric (V) acid (HNO_3) were all sourced from Kobian limited (outlet of Sigma Aldrich), Nairobi, Kenya. Distilled water obtained from Kenyatta University chemistry laboratory was used throughout the study.

Apparatus and instrumentation

The glassware were soaked in 10 % HNO_3 overnight and then scrubbed using a scotch brush, washed using hot water containing detergent, soaked in aqua regia (1 % HNO_3 / 3 % HCl) overnight, rinsed thoroughly with distilled water and air-dried. The instruments and equipment used were Thermogravimetric Analyzer (TGA-50 SHIMADZU), X-Ray Diffractometer (Rigaku MiniFlex II; Tokyo in Japan), Field Emission Scanning electron microscope (FEI ESEM, Vega3 Tescan LMH), Pulveriser rock grinding machine (Retsch RS 200), Automated X-Ray Fluorescence Spectrometer (Bruker S1 Titan 600, Tracer 5/ CTX), Fourier Transform Infrared Spectrophotometer (IR Tracer-100, Japan), Grinding mill (Retsch SR 200), Distiller (WSB 14), Magnetic stirrer with hot plate (WH240-HT), Drying oven (WTC binder FD53), Thermostat-controlled muffle furnace (MC5-12 Biobase) and Analytical weighing balance (ATX224 Shimadzu).

Sample collection

Sand samples were collected from the Bamburi beach (-3.98822'S, 39.73678'E) in Mombasa, Kenya, transported to Kenyatta University laboratories, pre-treated and stored in airtight container awaiting subsequent experiments. The coffee husk wastes were randomly collected in Othaya Constituency (-0.551751'S, 36.944703'E) in Nyeri County, cleaned using distilled water, chopped and oven-dried at 105 °C for 24 hours to remove moisture. The final material was then ground into a fine powder.

Silica extraction

The silica was extracted using a method described by Ndung'u *et al.* (2023). A 100.000 g of the sand powder was soaked in 6 N HCl solution in a glass beaker for 12 hours. The mixture was then filtrated, the residue washed with distilled water until there is no yellowish color and then dried at 105 °C to a constant weight. A 400 mL of 10 N NaOH solution was then added to the sand residue and heated at 150 °C while stirring for 4 hours. The filtrate (sodium silicate) was separated from the unreacted sand residues using Whatmann filter paper No. 1 and 6 N HCl solution slowly added to form a white gel (pH 7). The reaction mixture was left overnight at room temperature, filtered and rinsed with distilled water. The gel was then dried at 105 °C to a constant weight to obtain amorphous silica.

Biochar preparation

A 20 g of the biomass powder was first dried in an oven at 105 °C for 24 hours and a constant weight recorded. The pyrolysis was performed in a thermostat-controlled muffle furnace at a frequency of 50 Hz, 10 °C/min (heat rate), voltage of 220 V and power output of 3.0 kW. The powder was placed in a ceramic crucible and pyrolyzed at 300 °C for 5 hours (Fachini *et al.,* 2021). The biochar sample was allowed to cool, ground and weighed. The percentage yield was determined as the ratio of mass of biochar to mass of dried sample expressed as a percentage (Equation 2).

$$\text{Yield (\%)} = \frac{\text{Mass of biochar}}{\text{Mass of the dried sample}} \times 100 \quad (2)$$

Part of the obtained biochar was acid leached using 3 M HCl acid for 3 hours to remove any inorganic ash components (Alvarez *et al.,* 2016). The biochar material was then washed with distilled water to eliminate excess acid, oven-dried at 105 °C to a constant weight and stored in airtight bottles labelled CHB. The biochar sample was characterized using FT-IR, XRD, SEM and EDX.

The proximate analysis of the other part of the biochar samples was performed according to the gravimetric method of the ASTM (D1762-84) standard methods.

Silicon nitride (Si3N4) preparation

The preparation of silicon nitride adsorbents was carried out first by carbothermal reduction followed by nitridation process described by Maroufi *et al.* (2018) and Abdulhameed *et al.* (2018) with slight modifications. The process was performed using a digestion bomb locally made at Kenyatta University mechanical engineering laboratories, school of engineering. The bomb was made of a stainless steel (SS-316) whose cylindrical body was 105 mm in total length, 38 mm in external diameter, 23.5 mm in internal diameter. The top lid had a total length of 39 mm and thread length of 23.5×1.5×22 mm. The biochar powder was mixed with the extracted silica in the ratio of 3 to 2 for two hours and then placed in a digestion bomb. The bomb was tightly closed and placed in a thermostat-controlled muffle furnace and heated at 300 °C for 12 hours and the final product allowed to cool. Approximately 200 mL of NH_4OH solution (28 % v/v) was then added, bomb tightly closed and heating continued at 300 °C for another 12 hours. The final product was then allowed to cool, ground and stored in an airtight container awaiting characterization.

RESULTS AND DISCUSSION

Characterization of raw sand and extracted silica

XRD analysis

The XRD results for the raw sand (before and after acid treatment) and the extracted silica (ES) are shown by Figure 1.

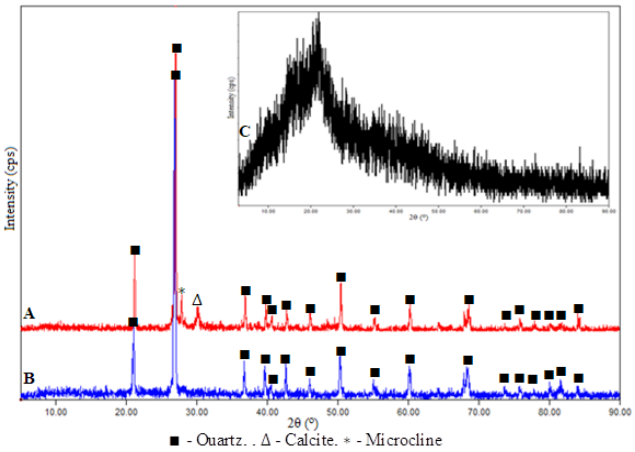

Figure 1: The XRD pattern of raw sand (A), acid-treated sand (B) and the extracted silica (C)

The results (diffractogram A) show that quartz (SiO_2) (JCPDS-ICDD file No. 46-1045), calcite ($CaCO_3$) (JCPDS-ICDD file No. 47-1743) and microcline (K (Al, Fe) Si_3O_8) (JCPDS-ICDD file No. 19-0932) are the main components of sand. A minor mineral phase of clinochlore ($(Mg, Fe)_6(Si, Al)_4O_{10}(OH)_8$)) (JCPDS-ICDD file No. 07-0078), although its crystal planes does not appear in the XRD patterns, is also suggested by the Match! software version 3.14 Build 238. A characteristic peak at 2θ 26.4 ° indicates the high crystallinity of the quartz phase (El-Sawy *et al.,* 2021). This is in agreement with the findings reported by Munasir *et al.* (2015) during their research study on the synthesis of SiO_2 nanopowders containing quartz and cristobalite phases from silica sands.

The peaks at 28.3 ° and 29.99 ° for microcline and calcite minerals disappeared in the acid treated sand (B). This implied that the purification process eliminated the major impurities in the sand to negligible amounts (Bousbih *et al.,* 2020). From the results in diffractogram C, a broad characteristic peak at 20.71° with the absence of any other intense peaks indicated the presence of a highly pure amorphous silica (JCPDS-ICDD file No. 001-0424). Also, the crystallite size was 31.84 nm showing that the silica was in nanoscale size (Ndung'u *et al.,* 2023).

XRF analysis

The chemical composition of the raw sand (BBS), acid treated sand (ABBS) and the extracted silica (ES) was determined by XRF. The results are presented in Table 1.

Table 1: Mean percentage of chemical composition of BBS, ABBS and ES

Sample	Oxide (%)					
	SiO_2	CaO	K_2O	Al_2O_3	Fe_2O_3	MgO
BBS	83.46 ± 0.39	6.48 ± 1.01	3.54 ± 0.14	2.62 ± 0.34	2.56 ± 0.07	0.99 ± 0.11
ABBS	88.14 ± 0.06	3.04 ± 0.03	0.12 ± 0.04	1.59 ± 0.22	1.95 ± 0.05	0.19 ± 0.04
ES	92.72 ± 0.63	0.25 ± 0.04	nd	0.09 ± 0.01	0.99 ± 0.09	nd

*nd – not detected

From the results in Table 1, the silica content of the raw sand was 83.46 ± 0.39 % with a low concentration of CaO (6.48 ± 1.01 %), K_2O (3.54 ± 0.14 %), Al_2O_3 (2.62 ± 0.34 %), Fe_2O_3 (2.56 ± 0.07 %) and MgO (0.99 ± 0.11 %). This showed that silica was the main component of the raw sand. The calcium oxide content could due to the presence of calcite ($CaCO_3$) mineral in the sand samples (Hachem *et al.,* 2023). The iron, magnesium, potassium and aluminium oxide contents could indicate the presence of minerals such as microcline (K (Al, Fe) Si_3O_8) and clinochlore $(Mg, Fe)_6(Si, Al)_4O_{10}(OH)_8$) in the silica matrix. This is in agreement with the XRD results.

The acid treatment of the sand samples increased the silica content to 88.14 ± 0.06 % while the amount of the other oxide components reduced. The purification process resulted to a mass decrease of the sand by 8.32 %. The yellowish-white colour was observed in the sand samples after acid treatment. This could be due to the residue iron contents in the acid-treated sand (Alyosef *et al.,* 2014). The results showed that the sand obtained were highly pure with minimal mass loss (< 10 %). The results are in agreement with those reported by Meftah *et al.* (2023) during their studies on extraction and physicochemical characterization of highly-pure amorphous silica nanoparticles from locally available dunes sand.

The analysis of the extracted silica shows that the silica content of 92.72 ± 0.63 % which corroborates the extraction of highly pure silica. The other oxide components were to negligible amounts. This showed that alkali fusion increased not only the silica content but also eliminated the remaining impurities that had remained in the sand after acid leaching (Munasir *et al.,* 2013).

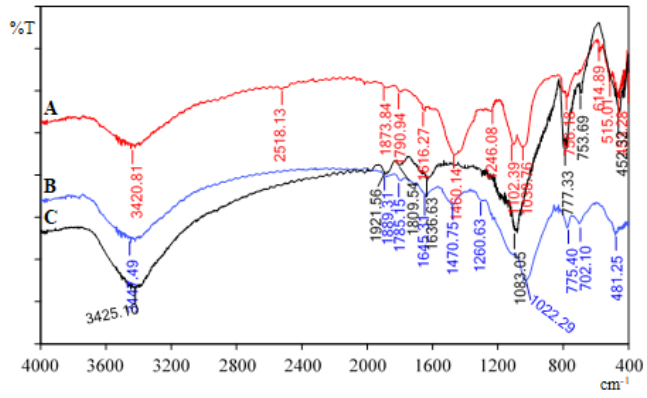

Figure 2: The FT-IR spectra of raw sand (A), acid-treated sand (B) and the extracted silica (C)

The results for the raw sand (A) shows a broak peak at 3420.81 cm^{-1} which was attributed to -OH stretch mode of water molecules in the sand (Zouaouid and Gheriani, 2018). This was confirmed by its flexion vibration at 1616.27 cm^{-1}. The peaks at 2518.13 cm^{-1} and 1460.14 cm^{-1} could be due to asymmetrical and symmetrical stretch vibrations of CO_3^{2-} groups (Meftah and Mahboub, 2019). This was confirmed by a peak at 1790.94 cm^{-1} attributed to the C=O stretch mode (Hachem *et al.,* 2023). This suggested the presence of calcite ($CaCO_3$) in the sand samples. The characteristic peaks at 1038.76 cm^{-1} and 756.18 cm^{-1} were ascribed to the Si-O-Si asymmetric and symmetric stretch vibrations (Yang *et al.,* 2023). Absorption bands observed at 614.89 cm^{-1} corresponded to Si-O-Fe and Si-O-Mg stretch vibrations (Beddiaf *et al.,* 2015). Also, at 515.01 cm^{-1} was a band for asymmetric Si-O-Al stretch vibrations (Abdelhak *et al.,* 2014). This could be due clinochlore and microcline mineral components in the silica matrix. The peaks at 453.28 cm^{-1} were associated with Si-O-Si bend mode (Yue *et al.,* 2018). The results confirm XRD and XRF results.

The FTIR spectrum for acid treated sand (B) showed peaks at 3447.49 cm^{-1}, 1645.31 cm^{-1}, 1022.29 cm^{-1}, 775.40 cm^{-1} and 481.25 cm^{-1} indicative of quartz in the sand. All the peaks showed shifting to higher or lower values. This could be influenced by reduction of impurities contained in the sample (Panwar *et al.,* 2015). The peak intensity for 1470.75 cm^{-1} and 1785.15 cm^{-1} was lower than that of the raw sand. Also, peaks at 2518.13 cm^{-1} disappeared after acid treatment. This showed that acid treating the raw sand decreased the calcite mineral contents in the sand samples. The peaks at 515.01 cm^{-1} and 605.66 cm^{-1} also disappeared after the acid treatment. The lost absorption bands showed elimination of the calcite, clinochlore and microcline impurities to lower amounts.

The FTIR spectrum of the extracted silica (C) showed peaks at 3425.10 cm^{-1} and 1636.63 cm^{-1} assigned to hydroxyl (OH^-) in silanol groups and/or adsorbed water molecules (Ndung'u *et al.,* 2023). Additionally, absorption bands at 1083.05 cm^{-1}, 777.33 cm^{-1} and 452.32 cm^{-1} correspond to the asymmetric, symmetric and bend vibration of Si-O-Si bonds respectively (Arunmetha *et al.,* 2015).

Biochar characterization

Proximate analysis

The percentage yield and proximate analysis of CHB was determined and results are tabulated in Table 2.

Table 2: Proximate analysis of the CHB

Analysis wt (%)	(Mean ± S.D)
Yield	25.11 ± 0.12
Moisture	7.45 ± 0.00
Volatile matter	74.80 ± 5.93
Ash	1.02 ± 0.27
Fixed carbon	16.73 ± 2.01

The results in Table 2 showed that a high volatile matter of 74.80 ± 5.93 % was released during the pyrolytic treatment of the raw biomass. This showed that all the volatiles trapped within the biomass matrix was eliminated forming biochar with a high carbon content (Bushra and Remya, 2020). The biochar had a carbon and ash content of 16.73 ± 2.01 % and 1.02 ± 0.27 respectively. The results indicated that the biochar obtained has a high carbon content and negligible ash content.

FT-IR analysis

The FT-IR analysis for both waste coffee husks and the char obtained by pyrolysis are shown in Figure 3.

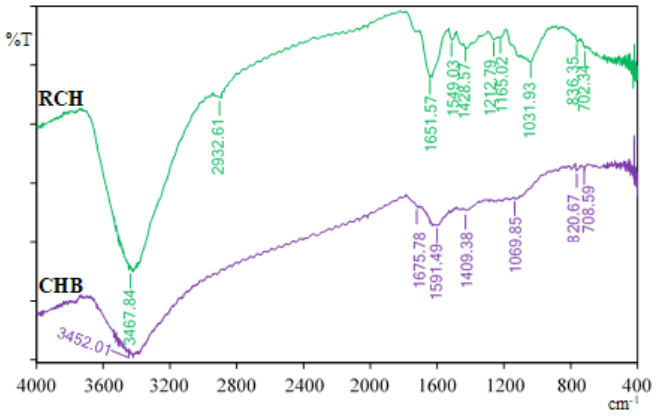

Figure 3: FT-IR spectra of raw coffee husk (RCH) and coffee husk biochar (CHB)

The results in FT-IR spectrum of the raw biomass showed a strong band at 3467.84 cm^{-1} which indicated bonded hydroxyl (-OH) groups. (Krishna Murthy *et al.,* 2020). The peak at 2932.61 cm^{-1} was attributed to CH_2 stretch mode in aliphatic groups (Alghamdi and El Mannoubi, 2021). The absorption peak at 1651.57 cm^{-1} correspond to carbonyl (C=O) groups stretch in carboxylic acid and its derivatives (Ndung'u *et al.,* 2021). The peak at 1549.03 cm^{-1} could be due to carbon-carbon (C=C) stretching vibrations of aromatic hydrocarbons (Mansuri *et al.,* 2018). This was confirmed by its bend mode at 836.35 cm^{-1}. The bands observed in 1212.79 cm^{-1} and 1031.93 cm^{-1} could be ascribed to C-O stretch vibrations of carboxylic acid derivatives and alcoholic groups (Nthiga *et al.,* 2021). The same peak at 1031.93 cm^{-1} together with a peak at 702.34 cm^{-1} could also be due to the stretching vibrations of Si-O-Si functional groups (Huljana *et al.,* 2021). The results confirmed the presence of silica in the raw biomass materials.

The methyl peak for the biochar FT-IR spectrum disappeared indicating the absence of the aliphatic carbon (Chen *et al.,* 2023). The spectrum showed a distinguished peak at 1591.49 cm^{-1} for C=C groups confirming the presence of aromatic carbon content (Kabayo *et al.,* 2019). The FT-IR spectrum didn't show any other major peaks which showed that there was complete pyrolysis of coffee husk wastes.

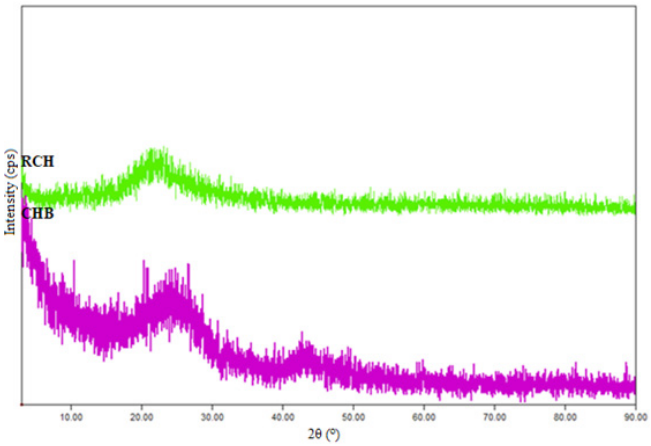

Figure 4: The XRD pattern of raw coffee husk (RCH) and coffee husk biochar (CHB)

The results in Figure 4 showed broad diffraction peaks at 21.97° showing that the raw biomass contains lignin, hemicellulose, pectin and cellulosic materials which are highly amorphous (Mu *et al.,* 2018). This corresponded to a diffraction peak for amorphous cellulose (JCPDS-ICDD file No. 03-0226). The same peak provides information on amorphous silica in the raw coffee husk biomass and its biochar (JCPDS-ICDD file No. 001-0424). The XRD diffractograms for CHB show diffraction patterns at 2α = 24.14° and 2α = 44.73° which correspond to the highly amorphous and diffuse graphite peaks (JCPDS-ICDD file No. 41-1487). This characterized a predominantly amorphous carbon structure (Jagdale *et al.,* 2019). There was no evidence of any inorganic phases in the XRD pattern showing that the prepared biochar sample had negligible ash content (Lawrinenko and Laird, 2015).

SEM analysis

The surface morphology of RCH and CHB was performed by Scanning Electron Microscope (SEM) at an accelerating voltage of 20.0 kV. The SEM micrographs obtained are presented in Figure 5.

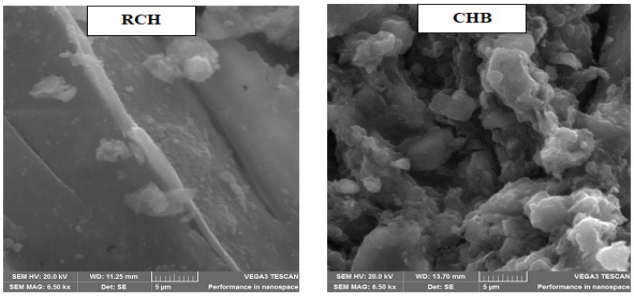

Figure 5: SEM micrograph for RCH and CHB

From the results in Figure 5, the SEM micrographs showed changes in the biochar surface texture and morphology before and after pyrolysis. The raw biomass surface structure was rigid, regular and less porous. After pyrolysis, the biochar surface became rugged and more porous. This is due to the rapid decomposition of volatile compounds during pyrolysis making the surface rougher and irregular (Sahoo *et al.,* 2020).

EDX analysis

The EDX spectra of raw coffee husk (RCH) and coffee husk biochar (CHB) are shown in Figure 6.

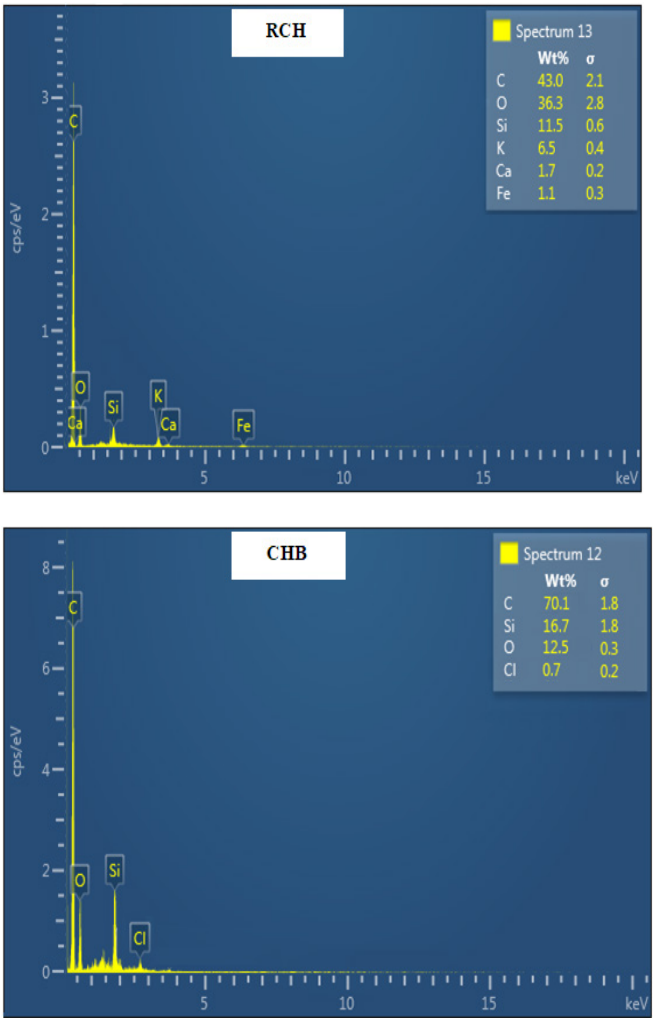

Figure 6: EDX spectra of RCH and CHB

From the results in Figure 6, the composition of RCH was 43.0 % (C), 36.3 % (O), 11.5 % (Si), 6.5 % (K), 1.7 % (Ca) and 1.1 % (Fe). The EDX spectrum showed the presence of carbon (C) and oxygen (O) as the main components of raw coffee husk. The elemental oxygen could also be as attributed to surface oxides of silica and metallic elements. The elemental composition of CHB was 70.1 % (C), 16.7 % (Si), 12.5 % (O) and 0.7 % (Cl). The final biochar showed a higher carbon and silica content with negligible ash contents comparatively to the raw biomass material. This showed that pyrolytic treatment followed by acid washing of the biochars not only decreased the inorganic ash contents from the biochar (Chang *et al.,* 2019) but also increased the carbon content. The chloride contents were detected in the final biochar material. This could be due to residue acid after the materials were washed with distilled water (Abdulhameed *et al.,* 2018).

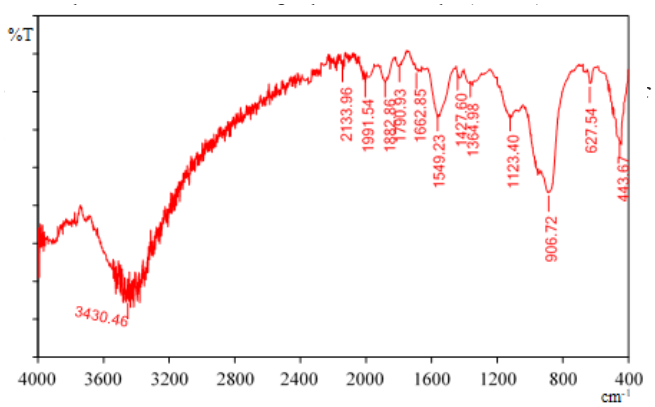

Figure 7: FT-IR spectrum of Si_3N_4

The FT-IR spectrum of the Si_3N_4 showed a broad peak at 3430.46 cm^{-1} corresponding to stretching vibrations of N-H and -OH of silanol (Si-OH) groups (Kobayashi, 2016). The peak at 1662.85 cm^{-1} could be due to OH^- bending vibration of silanol functional groups (Ramdani *et al.,* 2014). The absorbance peaks at 1549.23 $cm^{-1}$are indicative of the N-H bending modes (Shi *et al.,* 2014). The peaks at 1123.40 cm^{-1} could be ascribed to Si-O-C stretching vibration (Liang *et al.,* 2020). The bands at 906.72 cm^{-1} was ascribed to the Si-N-Si stretching vibrations (Jhansirani *et al.,* 2016). The peak at 627.54 cm^{-1} may correspond to a Si-Si stretching mode (Cui *et al.,* 2015). The absorption peak observed at 443.67 cm^{-1} was for Si-N stretching vibration in α-silicon nitride phase (Huang *et al.,* 2013).

XRD analysis

The XRD analysis of Si_3N_4 was performed at an applied current of 40 mA, accelerating voltage of 45 kV and the step size of 0.02. The diffractogram obtained is presented in Figure 8.

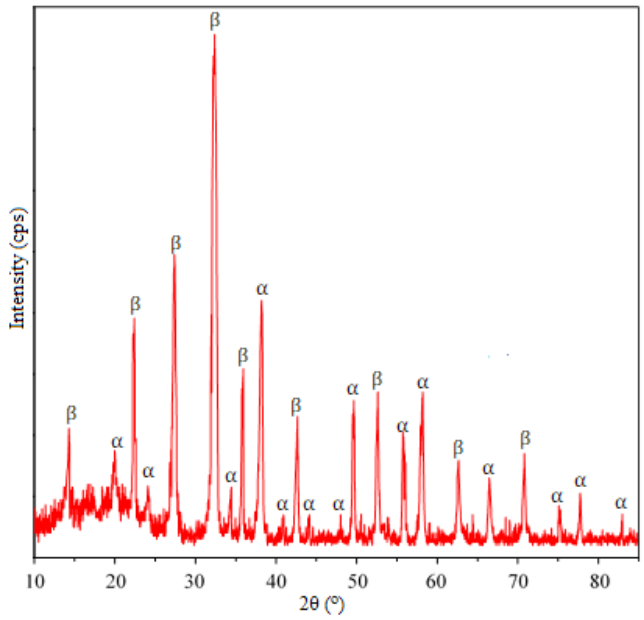

Figure 8: XRD spectrum of Si_3N_4

The XRD diffractogram (Figure 8) showed that Si_3N_4 was the main phase dominated by α-Si_3N_4 as major phase (JCPDS-ICDD file No. 41-0360) and α- Si_3N_4 (JCPDS-ICDD file No. 33-1160) as minor phase. The profile Rietveld analysis showed the relative amount of α-Si_3N_4 and α-Si_3N_4 phases in the Si_3N_4 composite was 68.97 % and 31.03 % respectively. The high yield content of α-Si_3N_4 phase could be due to the use of high purity amorphous raw materials for carbothermal reduction and nitridation at low temperatures (Ji *et al.,* 2014). The broad peak patterns in all the XRD spectra signified that the Si_3N_4 was predominantly amorphous (Biesuz *et al.,* 2019).

EDX analysis

The elemental composition of Si_3N_4 composite was determined using Energy Dispersive X-Ray (EDX) spectrometer. The spectrum is shown in Figure 9.

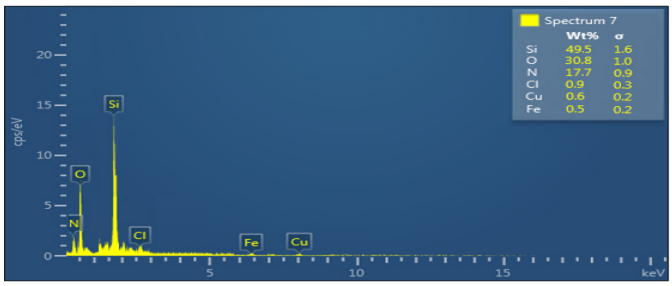

Figure 9: EDX spectrum of Si_3N_4

The results from EDX analysis showed that the elemental percentage composition of Si_3N_4 was 49.5 % and 17.7 % for silicon and nitrogen respectively. Minor peaks for copper observed could be due to contamination from the copper grid sample holder (Huang *et al.,* 2013). The oxygen content could be due to the silica residues and minor metal oxide components (Abdulhameed *et al.,* 2018) of biochar samples after acid leaching and/or Si_3N_4 surface oxidation during the analysis (Qadri *et al.,* 2016). The chloride contents were detected in the Si_3N_4 powder. This could be due to residue acid (Bariş, 2014) from the biochar samples used for synthesis of Si_3N_4.

TGA analysis

The Thermogravimetric analysis of Si_3N_4 was obtained at a varied temperature (0 °C - 600 °C), nitrogen gas flow rate (50 mL/min) and heating rate (15 °C/min). The TG curve is presented in Figure 10.

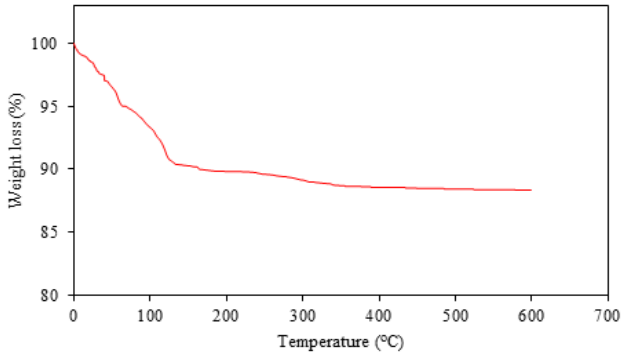

Figure 10: TG curve for Si_3N_4

The TGA curve for Si_3N_4 represents two weight change steps. At the first step from 0 °C to around 150 °C with a weight loss of 9.63 % beyond which no thermal effect is detected and the weight change is already achieved. This could be attributed to the vaporization of adsorbed water molecules onto the Si_3N_4 surfaces after which it remains stable (Qiu *et al.,* 2019). The mass profile was then flat until 600 °C implying that the Si_3N_4 material is thermally stable even at high temperatures.

CONCLUSION

The study prepared Si_3N_4 powder using silica extracted from Bamburi Beach sand (BBS) and biochar from coffee husk wastes in an ammonia environment. The XRD, XRF and FT-IR results showed that quartz (SiO_2), calcite ($CaCO_3$), clinochlore ($(Mg, Fe)_6(Si, Al)_4O_{10}(OH)_8$) and microcline (K (Al, Fe) Si_3O_8) as the main components of Bamburi Beach sand (BBS). The extracted silica contained silica as the main component (> 92 %), highly amorphous with hydroxyl (-OH) in silanol and siloxane (Si-O-Si) as important functional groups. The biochar samples obtained contained a porous carbon structure with aromatic carbon bonds (C=C) and a negligible ash content. The characterization of Si_3N_4 showed a porous composite with α-Si_3N_4 phase and α- Si_3N_4 phases. The material was thermally stable at varied temperatures with important functional groups of Silicon-Nitrogen-Silicon

(Si-N-Si), silanol (Si-OH) and Silicon-Nitrogen (Si-N). This greener approach is potentially applicable in utilizing silica and biochar from coffee husk waste materials as novel precursors for the synthesis of Si_3N_4 powder for industrial applications.

ACKNOWLEDGEMENT

The authors are grateful to Kenyatta University for laboratory space, chemicals, reagents, equipments, instruments and technical support.

REFERENCES

Abdelhak, M., Ahmed, K., Abdelkader, B., Brahim, Z. and Rachid, K. (2014). Algerian Sahara sand dunes characterization. *Silicon*, 6, 149-154.

Abdulhameed, A., Mbuvi, H., Changamu, E. and Maingi, F. (2018). Synthesis of silicon nitride from rice husk and sugarcane bagasse ashes. *Journal of Water technology and Treatment methods*, 1 (1), 106-111.

Alghamdi, W. and El Mannoubi, I. (2021). Investigation of seeds and peels of *Citrullus colocynthis* as efficient natural adsorbent for methylene blue dye. *Processes*, 9 (8), 1279-1297.

Alvarez, J., Lopez, G., Amutio, M., Bilbao, J. and Olazar, M. (2016). Preparation of adsorbents from sewage sludge pyrolytic char by carbon dioxide activation. *Process Safety and Environmental Protection*, 103, 76-86.

Alyosef, H., Ibrahim, S., Welscher, J., Inayat, A., Eilert, A., Denecke, R., Schwieger, W., Münster, T., Kloess, G., Einicke, W. Enke, D. (2014). Effect of acid treatment on the chemical composition and the structure of Egyptian diatomite. *International Journal of Mineral Processing*, 132, 17-25.

Anuar, M., Fen, Y., Emilia, R. and Khaidir, M. (2018) Synthesis and structural properties of coconut husk as potential silica source. *Results in Physics*, 11, 1-4.

Arunmetha, S., Karthik, A., Srither, R., Vinoth, M., Suriyaprabha, R., Manivasakan, P. and Rajendran, V. (2015). Size-dependent physicochemical properties of mesoporous nanosilica produced from natural quartz sand using three different methods. *RSC Advances*, 5 (59), 47390-47397.

Bakar, R., Yahya, R. and Gan, S. (2016). Production of high purity amorphous silica from rice husk. *Procedia Chemistry*, 19, 189-195.

Bariş, Y. (2014). Investigations of the productions of silicon nitride from Turkish rice husk. Thesis. The graduate school of natural and applied science, *Middle East University*.

Beddiaf, S., Chihi, S. and Leghrieb, Y. (2015). The determination of some crystallographic parameters of quartz, in the sand dunes of Ouargla, Algeria. *Journal of African Earth Sciences*, 106, 129-133.

Biesuz, M., Bettotti, P., Signorini, S., Bortolotti, M., Campostrini, R., Bahri, M., Ersen, O., Speranza, G., Lale, A., Bernard, S. and Sorarù, G. D. (2019). First synthesis of silicon nanoscrystals in amorphous silicon nitride from a preceramic polymer. *Nanotechnology*, 30 (25), 255601-255620.

Bousbih, R., Haddadi, I., Zina, H., Alatawi, N. and Ezzaouia, H. (2020). Purification of Tabuk silica using chemical attack and thermal treatment. *Journal of Non-Oxide Glasses*, 12 (3), 27-30.

Bushra, B. and Remya, N. (2020). Biochar from pyrolysis of rice husk biomass—characteristics, modification and environmental application. *Biomass Conversion and Biorefinery*, 10, 1-12.

Chang, R., Sohi, S.P., Jing, F., Liu, Y. and Chen, J. (2019). A comparative study on biochar properties and Cd adsorption behavior under effects of ageing processes of leaching, acidification and oxidation. *Environmental Pollution*, 254, 1-12.

Chen, C., Sun, K., Huang, C., Yang, M., Fan, M., Wang, A., Zhang, G., Li, B., Jiang, J., Xu, W. and Liu, J. (2023). Investigation on the mechanism of structural reconstruction of biochars derived from lignin and cellulose during graphitization under high temperature. *Biochar*, 5 (1), 51-64.

Cheng, Y., Luo, F., Jiang, Y., Li, F. and Wei, C. (2018). The effect of calcination temperature on the structure and activity of TiO_2/SiO_2 composite catalysts derived from titanium sulfate and fly ash acid sludge. *Colloids and Surfaces A: Physicochemical and Engineering Aspects*, 554, 81-85.

Cui, J., Li, B., Zou, C., Zhang, C. and Wang, S. (2015). Direct synthesis of α-silicon nitride nanowires from silicon monoxide on alumina. *Nanomaterials and Nanotechnology*, 5, 32-37.

Eddy, D., Puri, F. and Noviyanti, A. (2015). Synthesis and photocatalytic activity of silica-based sand quartz as the supporting TiO_2 photocatalyst. *Procedia Chemistry*, 17, 55-58.

El-Sawy, A., Gemeay, A.H., Helal, A.S. and Salem, M.A. (2021). Catalytic degradation of methylene blue in aqueous solution by H_2O_2 and SiO_2-NH_2-Cu(II)@SiO_2 nanoparticles as catalyst. *Journal of Molecular Liquids*, 341, 1-15.

Fachini, J., de Figueiredo, C., Joaquim, J., Rosa, S., da Silva, J. and do Vale, A. (2021). Novel K-enriched organomineral fertilizer from sewage sludge-

biochar: Chemical, physical and mineralogical characterization. *Waste Management*, 135, 98-108.

Farzana, R., Rajarao, R., Mansuri, I. and Sahajwalla, V. (2018). Sustainable synthesis of silicon nitride nanowires using waste carbon fibre reinforced polymer (CFRP), *Journal of Cleaner Production*, 188, 371-377.

Hasdemir, S., Tug˘rul, A. and Yilmaz, M. (2012). Evaluation of alkali reactivity of natural sands. *Construction and Building Materials*, 29, 378-385.

Hachem, R., Meftah, N. and Bouaziz, A. (2023). A comparative analysis of the microstructural and physicochemical properties of alluvial and dune sands from northeast Algerian Sahara. *The Journal of Engineering and Exact Sciences*, 9 (6), 1-14.

Huang, J., Huang, Z., Yi, S., Liu, Y., Fang, M. and Zhang, S. (2013). Fe-catalyzed growth of one-dimensional α-Si_3N_4 nanostructures and their cathodoluminescence poperties. *Scientific reports*, 3 (1), 1-9.

Huljana, M., Rodiah, S., Al Jabbar, J., Ichsan, C. and Marzuki, H. (2021). Silica-rice husk as adsorbent of Cr (VI) ions prepared through sol-gel method. *Walisongo Journal of Chemistry*, 4 (1), 65-73.

Jagdale, P., Ziegler, D., Rovere, M., Tulliani, J.M. and Alberto, T. (2019). Waste coffee ground biochar: A material for humidity sensors. *Sensors*, 19 (4), 801-816.

Jhansirani, K., Dubey, R., More, M. and Singh, S. (2016). Deposition of silicon nitride films using chemical vapor deposition for photovoltaic applications. *Results in Physics,* 6, 1059-1063.

Ji, H., Huang, Z., Chen, K., Li, W., Gao, Y., Fang, M., Liu, Y. and Wu, X. (2014). Synthesis of Si_3N_4 powder with tunable α/β-Si_3N_4 content from waste silica fume using carbothermal reduction nitridation. *Powder Technology*, 252, 51-55.

Jin, X., Xing, P., Zhuang, Y., Kong, J., Jiang, S. and Wei, D. (2019). Effect of Si_3N_4 diluent on direct nitridation of silicon powder. *Ceramics International*, 45 (8), 10943-10950.

Kabayo, S., Kindala, J., Nkanga, C., Krause, R. and Taba, K. (2019). Preparation and characterization of solid acid catalysts derived from coffee husks. *International Journal of Chemical Science*, 3 (6), 5-13.

Kobayashi, S. (2016). IR spectroscopic study of silicon nitride films grown at a low substrate temperature using very high frequency plasma-enhanced chemical vapor deposition. *World Journal of Condensed Matter Physics*, 6, 287-293.

Krishna Murthy, T., Gowrishankar, S., Krishna, R. H., Chandraprabha, M. and Mathew, B. (2020). Magnetic modification of coffee husk hydrochar for adsorptive removal of methylene blue: isotherms, kinetics and thermodynamic studies. *Environmental Chemistry and Ecotoxicology*, 2, 205-212.

Lawrinenko, M. and Laird, D.A. (2015). Anion exchange capacity of biochar. *Green Chemistry*, 17 (9), 4628-4636.

Liang, G., Sun, G., Bi, J., Wang, W., Yang, X. and Li, Y. (2020). Mechanical and dielectric properties of functionalized boron nitride nanosheets/silicon nitride composites. *Ceramics International*, 47 (2), 2058-2067.

Liu, H., Huang, Z., Zhang, X., Fang, M., Liu, Y., Wu, X. and Min, X. (2018). Large scale synthesis of α-Si_3N_4 nanowires through a kinetically favored chemical vapour deposition process. *Physica E*, 95, 132-138.

Mansuri, I., Farzana, R., Rajarao, R. and Sahajwalla, V. (2018). Carbon dissolution using waste biomass—A sustainable approach for iron-carbon alloy production. *Metals*, 8 (4), 290-301.

Maroufi, S., Mayyas, M., Nekouei, R., Assefi, M. and Sahajwalla, V. (2018). Thermal nanowiring of e-waste: A Sustainable route for synthesizing green Si_3N_4 nanowires. *ACS Sustainable Chemistry & Engineering*, 6 (3), 3765-3772.

Megawati, Fardhyanti, D., Putri, R., Fianti, O., Simalago, A. and Akhir, A. (2018). Synthesis of silica powder from sugarcane bagasse ash and its application as adsorbent in adsorptive-distillation of ethanol-water solution. *MATEC Web of Conferences*, 237, 1-6.

Meftah, N., Hani, A. and Merdas, A. (2023). Extraction and physicochemical characterization of highly-pure amorphous silica nanoparticles from locally available dunes sand. *Chemistry Africa*, 6, 1-10.

Meftah, N. and Mahboub, M. (2019). Spectroscopic Characterizations of sand dunes minerals of El-Oued (Northeast Algerian Sahara) by FTIR, XRF and XRD analyses. *Silicon*, 12 (1), 147-153.

Mu, B., Wang, H., Hao, X. and Wang, Q. (2018). Morphology, mechanical properties and dimensional stability of biomass particles/high density polyethylene composites: Effect of species and composition. *Polymers*, 10 (3), 308-322.

Munasir, Triwikantoro, Zainuri, M. and Darminto, (2015). Synthesis of SiO_2 nanopowders containing quartz and cristobalite phases from silica sands. *Materials Science-Poland*, 33 (1), 47-55.

Munasir, Sulton, A., Triwikantoro, Zainuri, M. and Darminto. (2013). Synthesis of silica nanopowder produced from Indonesian natural sand via alkali

fusion route. *American Institute of Physics*, 1555 (1), 28-31.

Ndung'u, S.N., Wanjau, R.N. and Nthiga, E.W. (2023). Facile extraction and characterization of silica nanopowder from marine national park beach sand via alkali fusion route. *International Journal of Technology*, 13, (1), 1-6.

Ndung'u, S., Nthiga, E., Wanjau, R. and Ndiritu, J. (2021). Adsorption studies of lead (II) ions from a synthetic media using Jackfruit (*Artocarpus heterophyllus L.)* rags: Kinetics, equilibrium and thermodynamic studies. *International Journal of Scientific Research in Chemical Sciences*, 8 (4), 5-12.

Norsuraya, S., Fazlena, H. and Norhasyimi, R. (2016) Sugarcane Bagasse as a renewable source of silica to synthesize santa barbara amorphous-15 (SBA-15). *Procedia Engineering*, 148, 839-846.

Nthiga, E., Ndung'u, S., Kibet, K. and Wanjau, R. (2021). Removal of Cr^{3+} ions from a model solution by HCl treated *Artocarpus heterophyllus* L. seeds: Equilibrium and kinetic study. *International Journal of Research and Innovation in Applied Science*, 6 (2), 38-45.

Pan, H. (2014). Ab *initio* design of nanostructures for solar energy conversion: a case study on silicon nitride nanowire. *Pan Nanoscale Research Letters*, 9, 531-539.

Panwar, K., Jassal, M. and Agrawal, A. (2015). In situ synthesis of Ag-SiO_2 anus particles with epoxy functionality for textile applications. *Particuology*, 19, 107-112.

Parrillo, A., Sánchez, G. and· Alles, A. (2021). α-Si_3N_4 and Si_2N_2O whiskers from rice husk and industrial rice husk ash. *SN Applied Sciences*, 3, 268-279.

Qadri, S., Rath, B., Gorzkowski, E., Wollmershauser, J. and Feng, C. (2016). Nanostructured silicon nitride from wheat and rice husks. *Journal of Applied Physics*, 119 (13), 1-7.

Qiu, B., Li, M., Xu, B., Liu, P., Chen, Q., Xu, B. and Han, Z. (2019). Effects of amino groups on dispersibility of silicon nitride powder in aqueous media. *Ceramics International*, 45 (4), 4268-4273.

Rajarao, R. and Veena, S. (2016). A cleaner, sustainable approach for synthesising high purity silicon carbide and silicon nitride nanopowders using macadamia shell waste. *Journal of Cleaner Production*, 133, 1277-1282.

Ramdani, N., Wang, J., Wang, H., Feng, T., Derradji, M. and Liu, W. (2014). Mechanical and thermal properties of silicon nitride reinforced polybenzoxazine nanocomposites. *Composites Science and Technology*, 105, 73-79.

Sahoo, K., Kumar, A. and Chakraborty, J.P. (2020). A comparative study on valuable products: bio-oil, biochar, non-condensable gases from pyrolysis of agricultural residues. *Journal of Material Cycles and Waste Management*, 23, 186-204.

Setyoningrum, T., Murni, S. and Nandari, W. (2020). Extraction of Silica from Kalirejo Minerals, Kokap, Kulonprogo, Yogyakarta. *LPPM UPN "Veteran" Yogyakarta Conference Series Proceeding on Engineering and Science Series*, 1 (1), 269-276.

Sharma, G., Kumar, A., Sharma, S., Naushad, M., Ahamad, T., Al-Saeedi, S., Al-Senani, G., Al-kadhi, N. and Stadler, F. (2018). Facile fabrication of $Zr_2Ni_1Cu_7$ trimetallic nano-alloy and its composite with Si_3N_4 for visible light assisted photodegradation of methylene blue. *Journal of Molecular Liquids*, 272, 170-179.

Shi, C., Zhu, Y., Qian, H. and Lu, L. (2014). Fabrication of silicon nitride fiber-PMMA composite through free radical polymerization in batch. *Materials Research Bulletin*, 51, 161-166.

Tran, C., Vu, H., Tran, N.V., Nguyen, N., Dang, K., Nguyen, A., Le, B., Mai, V., La, D., Phan, X. (2021). Synthesis of Si_3N_4 powder by powder metallurgy method in atmospheric pressure N_2: A review. *International Journal of Advanced Engineering Research and Science*, 8 (3), 31-37.

Vishnu, D., Sure, J., Kim, H., Kim, J., Kumar, R. and Schwandt, C. (2018). Direct electrochemical preparation of nanostructured silicon carbide and its nitridation behavior. *Journal of The Electrochemical Society*, 165 (14), D731-D742.

Wahyudi, A., Amalia, D. and Sariman. (2013). Preparation of nano silica from silica sand through alkali fusion process. *Indonesian Mining Journal*, 16 (3), 149-153.

Xiaohan, W. (2013). Carbothermal synthesis of Silicon Nitride. Thesis. School of Materials Science and Engineering. *The University of New South Wales*.

Yang, H., Mu, B., Zhang, T., Lu, Y. and Wang, A. (2023). Sustainable utilization of natural sands for cleaner preparation of high-performance nanostructured cobalt blue composite pigments by dolomite induced mechanochemistry. *RSC Sustainability*, 1, 1278-1289.

Yue, C., Liu, J., Zhang, H., Dai, L., Wei, B. and Chang, Q. (2018). Increasing the hydrophobicity of filter medium particles for oily water treatment using coupling agents. *Heliyon*, 4 (9), 1-14.

Zhao, Y., Shun Dong, S., Hu, P., Zhao, X. and Hong, C. (2021). Recent progress in synthesis, growth mechanisms, properties, and applications of silicon nitride nanowires. *Ceramics International*,

47 (11), 14944-14965.

Zouaouid, K. and Gheriani, R. (2018). Mineralogical analysis of sand roses and sand dunes samples from two regions of South Algeria. *Silicon*, 11 (3), 1537-1545.